Functional importance of JMY expression by Sertoli cells in mediating mouse spermatogenesis

Yue Liu[1,#], Jiaying Fan[1,2,#], Yan Yan[3], Xuening Dang[3], Ran Zhao[3], Yimei Xu[3], Zhide Ding[1,*]

[1] Department of Histology，Embryology, Genetics and Developmental Biology, Shanghai Key Laboratory for Reproductive Medicine, Shanghai Jiao Tong University School of Medicine, Shanghai 200025, China;

[2] Center for Experimental Medical Science Education, Shanghai Jiao Tong University School of Medicine, Shanghai 200025, China;

[3] Department of Clinical Medicine, Shanghai Jiao Tong University School of Medicine, Shanghai 200025, China

# Yue Liu and Jiaying Fan contributed equally to this work.

*Correspondence should be address to: Zhide Ding, *M.D., Ph.D.*, Department of Histology, Embryology, Genetics and Developmental Biology, Shanghai Jiao Tong University School of Medicine, No.280, Chongqing Road (South), Shanghai 200025, China.

Tel: +86-1391-6891-017, E-mail: zding@shsmu.edu.cn

Running title: Spermatid development depends on JMY expression

Abstract

Sertoli cells are crucial for spermatogenesis in the seminiferous epithelium because their actin cytoskeleton supports vesicle transport, cell junction, protein anchoring and spermiation. Here, we show that junction-mediating and regulatory protein (JMY), an actin regulating protein, also affects endocytic vesicle trafficking and Sertoli cell junction remodeling since disruption of these functions induced male subfertility in Sertoli cell-specific *Jmy* knockout mice. Specifically, these mice have: a) impaired BTB integrity and spermatid adhesion in the seminiferous tubules; b) high incidence of sperm structural deformity; c) reduced sperm count and poor sperm motility. Moreover, the cytoskeletal integrity in Sertoli cell-specific *Jmy* knockout mice was compromised along with endocytic vesicular trafficking. These effects impaired junctional protein recycling and reduced Sertoli cell junctions. In addition, JMY interaction with α-actinin1 and Sorbs2 was related to JMY activity and in turn actin cytoskeletal organization. In summary, JMY affects control of spermatogenesis through regulating actin filament organization and endocytic vesicle trafficking in Sertoli cells.

Key words: Sertoli cells, endocytic vesicle trafficking, junction-mediating and regulatory protein (JMY), junction remodeling, blood-testis barrier (BTB), spermatid development

Introduction

The testicular sustentacular cells, also known as Sertoli cells, are the only somatic cells in the seminiferous epithelium spanning the entire epithelium from the basement membrane into the lumen. They sustain a crucial nursing role through providing physical support, mediating nutrient transport, cleavage and eliciting paracrine signals that affect nascent sperm development (Griswold, 1998; França et al., 2016; Griswold, 2018). These functional roles help account for why sperm production critically depends on functional Sertoli cells interspersed within the seminiferous epithelial layer.

Cell to cell junctions between juxtaposed basal Sertoli cells surround the spermatogonia and delineate the boundary between the apical and basal seminiferous epithelium. These points of contact constituting the blood–testis barrier (BTB) include tight junctions, ectoplasmic specialization (ES), gap junctions and desmosome-like junctions (Mruk and Cheng, 2015). This physical barrier isolates the developing germ cells from immune responses to immune cell infiltration and exogenous toxins trapped in the basal compartment. Therefore, this barrier provides a molecule selectivity filter which creates a unique microenvironment supporting germ cell development (Mital et al., 2011; França et al., 2016; Stanton, 2016). Meanwhile, multiple germ cell–Sertoli cell junctions including desmosome-like junction and the ES, keep germ cells adhering to Sertoli cells. Moreover, the ES localized in the apical region of the Sertoli cells are critical for orienting the elongating spermatid and releasing them once they have developed into mature spermatozoa during spermiation

(França et al., 2016; Li et al., 2017). Therefore, the cell junctions elaborated by Sertoli cells, namely both Sertoli-Sertoli cell and Sertoli-germ cell junctions, contribute to sperm production in the seminiferous epithelium.

It is noteworthy that multiple junctions, particularly the tight junctions in Sertoli cells undergo dynamic restructuring during germ cell development. At stage VIII of the seminiferous epithelial cycle during spermatogenesis, preleptotene spermatocytes transit across the BTB near the basement membrane to promote the release of the adherent mature spermatid cells in the apical compartment wherein multiple junctions between adjacent Sertoli cells and Sertoli-germ cells instantaneously break down and then rapidly recombine. It is becoming clear that some tight-, gap-, adherens-, and desmosome-like junctional proteins undergo continuous endocytosis and recycling back to the plasma membrane, thereby resulting in scavenging of the old junctions and replacing them with new junctions (Mruk and Cheng, 2004; Du et al., 2013; Vogl et al., 2014). During this process, regulation of endocytic trafficking of junctional proteins provides a way of rapidly restructuring cell–cell junctions. Failure in any of these steps during endocytosis by Sertoli cells can lead to structural cell junctional defects in the seminiferous epithelium and subsequently an unstable environment for spermatogenesis (Cheng et al., 2011; Jia et al., 2017).

Endocytosis by Sertoli cells is regulated by androgens and cytokines (such as TNF-α, TGF-β2, TGF-β3, IL-6). Androgens can promote endosomal recycling and enhance formation of new cell junctions. In contrast, TGF-β, TNF-α and IL-6 linked signaling promote the fusion of endosomes to lysosomes, which enhances the

degradation of cell junctions (Yan et al., 2008; Su et al., 2010). Moreover, the actin cytoskeleton is essential for endocytosis and also for endosomal movement. Numerous studies demonstrated the important roles of both the actin cytoskeleton and actin regulating proteins in trafficking of junctional proteins and maintaining cell junction integrity in Sertoli cells (Li et al., 2016). For instance, recent studies showed that a class of actin-related proteins and their regulators, such as actin-related protein 3 (Arp3) and Wiskott-Aldrich syndrome protein (WASP), were involved in maintaining Sertoli cells tight junctions and BTB function (Lie et al., 2010; Xiao et al., 2014; Mok et al., 2015). More importantly, there are reports indicating that JMY, a junction-mediating and regulatory protein, is a member of the WASP family and it has a similar function to WASP and WHAMM (WASP homolog associated with actin, membranes, and microtubules). In addition, JMY is a multifunctional protein with roles in transcriptional co-activation of p53 and regulation of actin nucleation, which accompanies activation of the Arp2/3 protein complex (Roadcap and Bear, 2009). Analysis of the JMY protein sequence shows that its N-side contains a coiled-coil (CC) domain that can combine with the p300 protein. On the other hand, the C-side has three WASp Homology 2 (WH2) domains. They can combine with actin and a connector and an acidic (CA) domain and in turn with the Arp2/3 complex. When in the cytosol, JMY can activate Arp2/3 and produce branched F-actin filaments along with unbranched filaments via its tandem WH2 domains (Coutts et al., 2009; Zuchero et al., 2009; Rottner et al., 2010).

It is uncertain whether JMY has a functional role in mediating spermatogenesis

because its expression pattern has not been described in Sertoli cells. In addition, the effects are unknown of JMY protein downregulation or loss of function in Sertoli cells. Herein, we report that the JMY protein is highly expressed in Sertoli cells and is an actin regulator. This function is crucial in the maintenance of cell junction integrity which is vital for preserving spermatids adhesion and BTB integrity in Sertoli cells.

Results

Expression and localization of JMY in Sertoli cells

Immunofluorescent staining and immunoblotting detected JMY expression in the seminiferous epithelium of mouse testis and primary cultured Sertoli cells (Fig. 1 A, Fig. 2A, Fig. S1). JMY expression was prominent in Sertoli cells whereas it was much less evident in spermatids throughout the seminiferous epithelium (Fig. 1 A, Fig. S1). These results are consistent with Western blot analysis which also identified JMY expression in the testis and Sertoli cells (Fig. 2 A). Additionally, JMY was localized in the cytosol of cultured Sertoli cells and it was somewhat more evident at the F-actin-rich domain (Fig. 1 B), which is consistent with its actin-regulatory involvement.

Conditional knock out (CKO) of *Jmy* in the Sertoli cells

To identify the function of JMY in Sertoli cells, *Jmy* loxP mice were constructed. Accordingly, two loxP sites were inserted into the flanking regions of the third exon in the *Jmy* gene using homologous recombination (Fig. S2). Then, the *Jmy* flox (*Jmy*

133 $^{loxP/loxP}$) mice were mated with *Amh* cre mice in order to generate the expected Sertoli
134 cell specific *Jmy* CKO mice (*Jmy* $^{loxP/loxP}$; *Amh* cre^{+}). They carried a Sertoli cell
135 specific *Jmy* deletion which was obtained by splicing out exon 3 using the Sertoli cell
136 specific expression of Cre recombinase. In these *Jmy* CKO mice, Western blot and
137 immunofluorescent analysis documented that JMY testicular expression was absent in
138 Sertoli cells (Fig. 2 A and B), which confirms *Jmy* gene knockout in these mice.
139
140 **Reduced male fertility and poor sperm quality in *Jmy* CKO mice**
141 To assess the fertility of the *Jmy* CKO mice, each male was mated with two mature
142 females for one week and then litter sizes were compared with their wild type (WT)
143 counterpart. As expected, the litter size of male *Jmy* CKO mice (4.65 ± 1.31) was
144 significantly less than that of both the WT and the heterozygote (Het, *Jmy* lox/-) males
145 (WT: 7.40 ± 2.01, Het: 7.29 ± 0.95; Fig. 2 C). Moreover, the *Jmy* CKO sperm motility
146 and concentration also decreased in comparison with those of the WT and the Het
147 males (Sperm motility in WT: 65.60 ± 8.76, Het: 66.20 ± 6.58, CKO: 42.50 ± 5.74.
148 Sperm progressive motility in WT: 26.20 ± 5.89, Het: 23.80 ± 6.54, CKO: 16.50 ±
149 6.14. Sperm concentration, $\times 10^6$ per ml, in WT: 27.62 ± 7.82, Het: 23.54 ± 2.62,
150 CKO: 15.28 ± 4.41. Fig. 2 D and E), while the sperm head deformed ratios were
151 greatly enlarged (WT: 10.23 ± 3.38, Het: 14.60 ± 5.33, CKO: 43.65 ± 3.55. Fig. 2 F
152 and G). Thus, the reduced litter size and poor sperm quality clearly indicate that male
153 subfertility was established in the *Jmy* CKO mice.
154

155 **Morphological alteration in *Jmy* CKO testes**

156 The testicular morphology of *Jmy* CKO mice was abnormal compared to that in the
157 WT and the Het counterparts. The *Jmy* CKO testes had asyntactic Sertoli cells at the
158 basal region of the seminiferous epithelium and poor adhesion between spermatids
159 and Sertoli cells, leading to the abscission of round spermatids into the lumen of
160 seminiferous tubules (Fig. 3 A), whereas in the sections of *Jmy* CKO caput
161 epididymis, masses of round spermatids were evident in the epididymal duct lumen
162 (Fig. 3 B).

163 To characterize the cell type alterations in the seminiferous epithelium, cell cycle
164 analysis was performed in *Jmy* CKO and WT mice. The cell types were classified
165 according to karyotype analysis based on comparing spermatogonia, secondary
166 spermatocyte and Sertoli cells of diploid cells with those of: a) primary tetraploid
167 spermatocytes in the tetraploid cells; b) haploid spermatids and spermatozoa. The
168 results revealed a significantly higher percentage of haploid cells in *Jmy* CKO
169 seminiferous epithelium compared to that in the WT seminiferous epithelium (Fig. 3
170 C). Meanwhile, the number of Sertoli cells was evaluated based on the
171 immunostaining expression pattern of vimentin, which is a Sertoli cell marker, in 8
172 weeks old *Jmy* CKO and WT mice. The number was essentially the same between
173 these two groups (Fig. 3 D).

174 Additionally, electron micrographs showed that cell adhesions were
175 unconsolidated within the seminiferous epithelia of the *Jmy* CKO testes (Fig. 3
176 E), and junctional structures between the Sertoli cells, especially the actin bundles of

177 the ES were greatly disrupted (Fig. 3 F).

178 The in vivo classical biotin permeation assay compared the BTB integrity in the
179 *Jmy* CKO with that in the WT and Het testes. As expected, the staining patterns
180 clearly defined basal spermatogonia but none were present in the upper apical cell
181 layers in the WT and Het testes. In contrast, biotin readily permeated throughout the
182 entire germinal epithelium in the *Jmy* CKO testes (Fig. 3 G).

183 In summary, loss of *Jmy* in Sertoli cells impaired Sertoli cell junctional barrier
184 formation and loosened spermatid attachment.

185

186 **Disrupted cell junctions and endocytosis in *Jmy* CKO testes**

187 To confirm the alteration of cell junctions in *Jmy* CKO testes, immunoblot analyses
188 evaluated junctional signature protein expression. ZO-1, claudin11 (tight junction
189 proteins), as well as β-catenin (adherens junction protein) expression levels decreased
190 in the *Jmy* CKO testes in comparison to those in WT testes (Fig. 4 A). Meanwhile,
191 immunohistochemistry analyses showed that expression of N-cadherin, specifically
192 localized in the basolateral region of adjacent Sertoli cells in WT testes decreased and
193 was more diffuse in the junctional compartment of Sertoli cells in *Jmy* CKO testes
194 (Fig. 4 B). Thus, these results show that the declines in expression of cell junctional
195 proteins impaired tight junctioncontacts and BTB integrity between neighboring
196 Sertoli cells in the *Jmy* CKO testes.

197 Notably, dynamic trafficking of tight junctionproteins is crucial for maintaining
198 barrier function and it is greatly dependent on endocytosis. Endocytic trafficking of

junctional proteins, including continuous endocytosis and recycling back to the plasma membrane enables rapid junctional remodeling. Immunoblot analysis of clathrin (an endocytic vesicle marker) and EEA-1 patterns (an early endosomal marker) showed that they increased in *Jmy* CKO testes (Fig. 4 A). These changes indicate that decreased levels of junctional protein expression may result from endocytosis up-regulation in *Jmy* CKO testes.

Disrupted cell junctions and endocytosis in *Jmy* CKO Sertoli cells

Primary cultured Sertoli cells were used to confirm that alterations in cell junctional integrity and endocytosis occur in *Jmy* CKO mice. As stated above, immunoblot analyses showed that the tight junction protein (occludin) and the adherens junction proteins (β-catenin and N-cadherin) were downregulated in *Jmy* CKO Sertoli cells. In contrast, the endocytic vesicle markers (clathrin and caveolin 1), the early endosomal marker (EEA-1) and the recycling endosome marker (Rab 11) were upregulated in *Jmy* CKO Sertoli cells, whereas the later endosome marker (Rab 7) was unchanged in *Jmy* CKO Sertoli cells (Fig. 4 C). Immunofluorescent staining analyses of cultured Sertoli cells also confirmed declines in N-cadherin and ZO-1 localization at the cell–cell interface of *Jmy* CKO Sertoli cells, as well as the increases in contents of caveolin 1 and clathrin in *Jmy* CKO Sertoli cells (Fig. 4 D). These findings unequivocally confirm losses in cell junctional formation whereas endocytosis increased in *Jmy* CKO Sertoli cells. These changes suggest that JMY expression contributes to controlling endocytic trafficking of junctional proteins.

Another indication of JMY involvement is that treatment of normal WT Sertoli cells with dihydrotestosterone (DHT), markedly upregulated clathrin, an activator of endocytosis and endosome recycling, and EEA-1 and Rab11 endocytosis related proteins. These changes are consistent aforementioned indications of JMY involvement in controlling BTB integrity and endocytic trafficking. Likewise, upon treatment of WT Sertoli cells with dynasore, an inhibitor of dynamin and vesicle trafficking, the contents of junctional proteins, i.e. occludin, β-catenin and N-cadherin significantly decreased, which is also consistent with their alterations in *Jmy* CKO Sertoli cells (Fig. 4 C). Therefore, the effects of loss of JMY function on Sertoli cells are similar to those induced by DHT and dynasore treatments. This correspondence strengthens the notion that JMY is involved in endocytic vesicle trafficking and endosomal recycling.

Disrupted endosomal cycling in *Jmy* CKO Sertoli cells

Endocytosis occurs through multiple steps which initially include internalization of proteins spanning the entire width of the plasma membrane followed by vesicular trafficking into early endosomes. Subsequently, the endosomes are inserted into the lysosomal degradative pathway or recycled back to the plasma membrane. To identify the trafficking fate of the endocytosed junctional proteins, we used a biotinylation assay that labels extracellular amino residues of membrane proteins and allows their trafficking to be monitored. In WT Sertoli cells, the biotin labeled proteins were initially detected at the surface of cells and endocytosis gradually moved them into the

cytoplasm. Because DHT induces endosomal recycling, the biotin labeled proteins recycled back to the plasma membrane of Sertoli cells at the cell-cell interface after either 1 hour or 3 hours culture in vitro (Fig. 5 A). Even though biotin-labeled membranous proteins were transported into the cytoplasm by endocytosis in *Jmy* CKO Sertoli cells, endocytic trafficking was not completed since the proteins accumulated in the cytoplasm (Fig. 5 A). Alternatively, treating with dynasore blocked endocytosis at a step prior to biotin labeling in *Jmy* CKO Sertoli cells, thus the biotin labeled membranous proteins remained on the cell surface (Fig. 5 B).

Moreover, immunofluorescent staining also demonstrated that a large amount of biotin labeled proteins accumulated in the cytoplasm of *Jmy* CKO Sertoli cells and colocalized with endocytic vesicle markers, clathrin and caveolin 1, rather than the endosomal markers, EEA-1 and Rab 11 (Fig. 5 C). These results suggest that the loss of *Jmy* function blocks vesicle trafficking into the early endosomes.

Identification of proteins interacting with JMY by immunoprecipitation (IP) and liquid chromatography tandem mass spectrometry (LC-MS) analysis

Due to the role of JMY as an actin regulator, we hypothesized that cooperative interaction between JMY and some other proteins contribute to endocytic vesicle trafficking. To gain insight into the molecular mechanism underlying JMY effects on vesicle trafficking, the proteins interacting with JMY in Sertoli cells were separated by IP and then identified by LC-MS analysis (Table S1). Kyoto Encyclopedia of Genes and Genomes (KEGG) databases (http://www.genome.jp/kegg/) was used to

analyze the MS data in order to search for functional annotation terms and pathways. The analysis showed that the proteins interacting with JMY are mainly constituents of a group classified as “Regulation of actin cytoskeleton”, “Tight junction”, “Focal adhesion” and “Endocytosis” in Sertoli cells (Table S2). Similarly, Clusters of Orthologous Groups of proteins (COG) analysis revealed that 15 proteins identified by MS were classified as “Cytoskeleton” (Fig. S3). Considering the known actin-regulating activity of JMY, such we were prompted to determine if it interacts with these other actin cytoskeleton related proteins. Within this group, drebrin, actin-related protein 2/3 complex (Arp2/3), Anxa2, Cofilin, Gelsolin, spectrin have been reported to participate in regulating cell junction formation and function in Sertoli cells (Guttman et al., 2002; Lui et al., 2003; Lie et al., 2010; Li et al., 2011; Aristaeus de Asis et al., 2013; Chen et al., 2017; Chojnacka et al., 2017).

Previous studies demonstrated that the WH and CA domains of JMY bound to the actin and Arp2/3 complex to promote actin nucleation (Coutts et al., 2009; Zuchero et al., 2009; Rottner et al., 2010). Herein, our analysis predicted that JMY interacts with the Arp2/3 complex as well as other actin binding protein candidates that include α-actinin1, Sorbin and SH3 domain containing protein 2 (Sorbs2) in Sertoli cells. If this prediction proves to be valid, the structure of the actin and Arp2/3 complex may in fact also contain other constituents.

Verification of interactions between JMY and two actin binding proteins, α-actinin1 and Sorbs2

Since α-Actinin1 and Sorbs2 very prominently interact with JMY based on their presence in immunoprecipitates of JMY, we presumed that they support JMY function by serving as its co-factors. To confirm such an interaction, we interrogated immunoblots obtained with JMY antibodies for both α-actinin1 and Sorbs2. Their presence in the JMY immunoprecipitates shown in Figure 6A documents that JMY interacts with α-actinin1 and Sorbs2.

Furthermore, immunofluorescent staining substantiates α-actinin1 and Sorbs2 colocalization in cultured Sertoli cells. The images clearly show that they are present in close proximity to the actin cytoskeleton. More importantly, JMY colocalizes at the cell edges with this complex formed between α-actinin1 and Sorbs2 and the actin cytoskeleton network (Fig. 6 B). Colocalization of JMY with these proteins strengthens the notion that these proteins bind to JMY. Accordingly, it is possible that they may interact with one another and mediate specific biological functions such as endocytosis.

Differential expression of α-actinin 1 and Sorbs2 in *Jmy* CKO Sertoli cells

JMY involvement in fostering a structured actin network was confirmed by the fact that rhodamine-phalloidin stained actin filaments were disordered with highly branched and extensive foci in *Jmy* CKO Sertoli cells (Fig. 7 A). Nevertheless, the expression and localization of Arp3 in *Jmy* CKO Sertoli cells were clearly unchanged from those in WT Sertoli cells (Fig. 4 C, Fig. 7 B and C). This invariance suggests that the disorganized and unstructured actin cytoskeleton induced by loss of *JMY*

function was not dependent on an interaction between JMY and Arp2/3.

Although both α-actinin1 and Sorbs2 strongly interact with the actin cytoskeleton, their relationship to JMY function required clarification. Notably, in *Jmy* CKO Sertoli cells, both the α-actinin and Sorbs2 expression levels detected by immunoblotting were slightly reduced (Fig. 7 B). A more striking change was that loss of JMY function caused α-actinin 1 and Sorbs2 to lose their close proximity to one another. This disruption is evident based on the altered immunofluorescent staining pattern showing disorganization of the actin cytoskeletal filament network (Fig. 7 A). What is even more informative is that changes in their immunofluorescent staining pattern was delocalized and accompanied disordering of the actin filament organization (Fig. 7 C). Taken together, it is apparent that JMY expression is essential for positioning α-actinin1 and Sorbs2 in locations that are commensurate for mediating development of an organized actin cytoskeleton network.

Discussion

There is suggestive evidence that the actin cytoskeleton and its binding proteins play an important role in maintaining Sertoli cell function and supporting BTB integrity and spermiogenesis. Here we identify a novel role for JMY, which is an actin regulating protein. It is an essential factor for enabling dynamic remodeling of the junctional proteins mediated by endocytic trafficking in Sertoli cells. JMY involvement in this process is evident because loss of *Jmy* function impaired BTB structural and integrity formation in Sertoli cells, which is obligatory for preventing

premature sloughing of developing germ cells from the seminiferous epithelium. Such protection is necessary because it prevents dysfunctional sperm development from reducing sperm fertility as a consequence of declines in sperm count and motility that is associated with a high incidence of sperm head structural deformity.

Sertoli cells are rich in actin filaments, which play a crucial role in certain biological activities, e.g., vesicle transport, ES formation and spermatid head shaping (Du et al., 2013; Vogl et al., 2014; Li et al., 2016; Li et al., 2017). Our results indicate that the JMY distribution pattern is reflective of a possible association between changes in JMY expression and dynamic modulation of the actin cytoskeleton. Specifically, JMY expression was evident in the Sertoli cells and later-stage spermatogenic cells in the seminiferous epithelium. JMY expression exhibited a filament-like expression localized parallel to the actin filaments in Sertoli cells, whereas in the later-stage spermatogenic cells, it was specifically localized in the perinuclear ring and manchette structure which was also rich in actin filaments. Such observations suggested that JMY is likely involved in mediating actin-regulating activity during spermatogenesis. Accordingly, we undertook a characterization of the underlying molecular mechanisms mediating JMY function in spermatogenesis.

To determine the contribution by JMY expression in either Sertoli cells or spermatogenic cells to spermatogenesis, we engineered mice both with Sertoli cell-specific deletion of *Jmy* (*Jmy* flox; *Amh* cre) and germ cell-specific deletion of *Jmy* (*Jmy* flox; *Mvh* cre). Even though the mice with germ cell-specific deletion of *Jmy* were healthy and fertile (Fig. S4), male mice with Sertoli cell-specific deletion of

353 *Jmy* were sub-fertile. This condition was attributable to low sperm count and poor
354 sperm motility as well as appreciable morphological deformity. Disruption of BTB
355 integrity accompanying loss of *Jmy* function could account for declines in sperm
356 fertility since reduced barrier function led to premature sloughing of developing
357 spermatids.

358 In Sertoli cells, junctional structures undergo extensive organization and transition
359 between “close” and “open” configurations to facilitate transport of germ cells across
360 the BTB as well as control spermatid adhesion or sperm release. This dynamic
361 remodeling of cell junctional barrier function greatly depends on endocytosis and
362 linked endocytic trafficking pathways, which select the endocytosed proteins to be
363 sorted for degradation or recycling (Cheng et al., 2011; Vogl et al., 2014). Moreover,
364 ES is a unique actin-based cell-cell anchoring junction constituted by bundles of actin
365 filaments that are situated between the cisternae of the endoplasmic reticulum and the
366 apposing plasma membrane. In general, these structures are restricted to the interface
367 between Sertoli cells and spermatids and are designated as the apical ES. On the other
368 hand, those located at the Sertoli-Sertoli cell interface are referred to as the basal ES,
369 which usually coexists with tight junctions and gap junctions to constitute the BTB
370 structure. Interestingly, germ cell transport as well as endocytic vesicle trafficking in
371 Sertoli cells requires rapid reorganization of these microfilament bundles, so that they
372 are efficiently converted from a “bundled” to “unbundled /branched” configuration
373 (Li et al., 2015). Briefly, there is no doubt that irrespective of the type of actin bundle
374 configuration, in all cases they support and maintain cell junction integrity. On the

other hand, actin branching is a critical step weakening cell junction cohesiveness resulting in junctional reorganization in the seminiferous epithelium. Our electron microscopy analysis confirmed that these alterations occurred in the *Jmy* CKO seminiferous epithelium. Notably, the junctional BTB structures appeared disfigured and actin filament bundle density declined at the basal ES. Such changes cause the BTB to become more permeant resembling those in more leaky epithelia and endothelia. Furthermore, the phalloidin stained actin filaments of *Jmy* CKO Sertoli cells were in disarray having highly branched and enlarged as well as more numerous foci, suggesting that JMY might be essential as well for the maintenance of the effective bundled actin filaments and the ES junctions in Sertoli cells. These changes may also explain why loss of JMY function disrupts cell junction formation; namely, it occurs as a consequence of actin branching.

Additionally, we found that loss of *Jmy* function in Sertoli cells reduced expression of junctional proteins (i.e. ZO-1, claudin11, N-cadherin, occludin and β-catenin) and increased expression of endocytosis related proteins (i.e. clathrin, caveolin 1, EEA-1 and Rab 11) both in the testis and in the Sertoli cells. These effects are tentatively supportive of a mechanism, which links impaired cell junctions and BTB formation with abnormal endocytosis in Sertoli cells. To evaluate this possibility, the effects of testosterone (DHT) treatment or dynasore treatment were determined in an in vitro Sertoli cell culture system since these agents can increase or decrease BTB resistance, respectively and thereby mimic their dynamic behavior in vivo. Our usage of these modulators is based on reports in which testosterone promoted cell junction

integrity, apparently via enhancing protein endocytosis and recycling, while dynasore, a well-characterized dynamin inhibitor effectively blocks endocytosis and vesicle trafficking. In our case, testosterone treatment of WT Sertoli cells induced both endocytosis and endosome recycling, whereas dynasore treatment impeded endocytosis, which subsequently impaired cell junction formation. These opposing effects were similar to those occurring in *Jmy* CKO Sertoli cells. Therefore, the loss of JMY function disorders endocytosis which in turn impairs BTB cell junction formation in Sertoli cells.

The biotinylation assay was performed to confirm that loss of JMY function does indeed disorganize endocytosis. With this procedure, membrane protein endocytosis was visualized in Sertoli cells. The results provide the first evidence that membrane proteins are continuously endocytosed and recycled back to the cell surface, resulting in an enhanced biotinylated barrier at the cell–cell interface. JMY involvement in this process was clearly documented by showing that the loss of its function interrupted endocytosis by causing the internalized protein to accumulate in the cytoplasm rather than translocate into early endosomes. Interestingly, our results indicate that JMY expression is not required for plasma membrane internalization but it is essential for endocytosed vesicle trafficking into early endosomes. Notably, the actin cytoskeleton is reported to play an important and variable role in vesicular transport (Liu, 2016; Papadopulos, 2017). This realization supports the notion that JMY induced vesicle trafficking is mediated through JMY interacting with the actin cytoskeleton.

Our protein interaction analyses provide other indications that JMY along with

419 other actin binding proteins (i.e. Arp3, Sorbs2, α-actinin1) cooperate with each other
420 to perform specific functions in Sertoli cells. One of them includes the Arp2/3
421 complex which JMY activates and produces branched F-actin filaments. Moreover,
422 the Arp2/3 complex modulates invagination and pinching off of endosomes. They are
423 then delivered to sorting endosomes as well as actin branches to promote BTB
424 structural reorganization in a number of different vesicle-trafficking pathways (Lie et
425 al., 2010). Remarkably, JMY was capable of nucleating actin filaments in either the
426 presence or absence of the Arp2/3 complex (Zuchero et al., 2009). Herein, our results
427 indicate that the effect of JMY on the actin cytoskeleton seems to be independent of
428 the Arp2/3 complex in Sertoli cells. Its protein interaction might instead depend on its
429 three WH2-domains that interact with other proteins.

430 To determine if this speculation is credible, IP and MS analysis were performed
431 and revealed that JMY could interact with Sorbs2 and α-actinin1 in Sertoli cells.
432 Sorbs2 (also known as Arg Kinase-binding Protein 2, ArgBP 2), contains an
433 N-terminal SoHo (Sorbin homology) domain and three conserved SH3 domains in the
434 C-terminal region. It has been reported to associate with actin fibers, adherens
435 junction and tight junctions, and is involved in actin cytoskeletal organization, cell
436 adhesion and migration (Roignot and Soubeyran, 2009). On the other hand, α-actinin1
437 (ACTN 1) is one of the major actin cross-linking proteins and anchors actin filaments
438 to junctional structures and has an important role in some cellular biological processes
439 such as cytokinesis, cell adhesion and cell migration (Murphy and Young, 2015).
440 Recent evidence implicates that Sorbs2 can interact with α-actinin, subsequently

binding to actin filaments (Rönty et al., 2005; Anekal et al., 2015). The current study is the first one describing interactions between the α-actinin1, Sorbs2 and JMY triad in Sertoli cells. Such interactions are consistent with our identification of colocalization of JMY with Sorbs2 and α-actinin1 along the peripheral edges of Sertoli cells. This delimited expression was particularly evident proximal to the nuclei. These regions demarcate the basal region which delineates both Sertoli cell polarity and the boundary between the uppermost apical and basal regions constitutes the BTB. Additionally, loss of *Jmy* function could lead to disordered distribution of Sorbs2 and α-actinin1, suggesting a critical role played by JMY in cross-linking the actin-related proteins to actin filaments.

In conclusion, JMY, an actin regulating protein, is essential for mediating dynamic remodeling of the BTB junctional proteins in Sertoli cells. It involvement in this process is requisite for the recycling phase of endocytic trafficking. Accordingly, JMY is crucial for sustaining the BTB structural organization commensurate with sperm health and male fertility.

Materials and methods

Animals

C57BL/6 mice were purchased from Shanghai Laboratory Animal Center. Anti-Mullerian hormone (*Amh*)-Cre mice (Jax number 007915) and *Jmy*-loxP mice (the *Jmy* exon 3 flanked by 2 loxP sites) were from Shanghai Research Center For Model Organisms (Shanghai, China). All of the mice were acclimated in the Animal

Center of Shanghai Jiao Tong University School of Medicine. Animal experiments were conducted according to the International Guiding Principles for Biomedical Research Involving Animal, as promulgated by the Society for the Study of Reproduction. This research program was approved by the ethics committee of Shanghai Jiao Tong University School of Medicine (NO. A2015-034).

Fertility evaluation

Individually housed, sexually mature male mice (8 weeks old) cohabitated with two virgin female mice (10 weeks old) for 7 days, and they were then separated from one another. Every day during cohabitation, females were examined for vaginal plugs as evidence of mating. Approximately, 20 days after the last day of cohabitation, the number of pups delivered by each mated female mouse was counted and the litter sizes were analyzed.

Sperm parameters analyses

The cauda epididymides were dissected and then placed in pre-warmed (37°C) Tyrode's Buffer (Sigma-Aldrich) to allow dispersion of spermatozoa. After 15 minutes, sperm motility, progressive motility and concentration were analyzed by computer-assisted sperm analysis (CASA) (Hamilton Thorne).

For teratozoospermia analysis, a sperm pellet was initially smeared on a glass slide. After reaching dryness at room temperature, the slide was fixed and stained as described in the Diff-Quick method (BRED Life Science Technology Inc., China).

485 The slide was viewed under a microscope (Olympus BX53) equipped with an
486 UPlanFN N 40×/0.75 objective (Olympus).
487
488 **Tissue preparation**
489 Mice were euthanized with CO_2 and then their testis and epididymis were removed.
490 For RNA analysis, tissue was immediately snap frozen in liquid N_2. For histological
491 analysis, tissues were fixed overnight either in Bouin's solution or in 2.5%
492 glutaraldehyde buffer for electron microscopy analysis.
493
494 **Histological Analysis**
495 Testes and epididymis fixed in Bouin's solution were embedded in paraffin, and
496 specimens were sliced into 5 mm thick sections and mounted on glass slides, followed
497 by deparaffinization and rehydration. The sectioned testicular and epididymal tissues
498 were then stained with hematoxylin and eosin (H&E) and observed under a
499 microscope (Olympus BX53) equipped with an UPlanFN N 20×/0.5 objective and an
500 UPlanFN N 40×/0.75 objective (Olympus).
501
502 **Transmission electron microscopy analysis**
503 Small pieces of testicular tissue were immersed in 2.5% glutaraldehyde solubilized in
504 0.1M phosphate buffer (pH 7.4) for 1 day. The tissues were then fixed in 1% osmium
505 tetroxide and dehydrated through a graded ethanol series, and embedded in Epon 618
506 (TAAB Laboratories Equipment). Ultra-thin sections (70-90 nm) in the seminiferous

507 epithelium region were stained with lead citrate and uranyl acetate, and then
508 examined at 100 kV with a Philips CM-120 (Philips).
509
510 **Western blot analysis**
511 Mice testes or cultured cells were homogenized in RIPA lysis buffer (Thermo Fisher
512 Scientific) containing protease inhibitor cocktail (Roche) on ice for 30 min followed
513 by centrifugation at 12,000 xg, for 10 min, at 4°C. The proteins in the supernatant
514 were collected and the protein concentrations were determined by the BCA Protein
515 Assay Kit (Thermo Fisher Scientific).
516 Protein samples (20 μg) were separated using 8% – 16% denaturing
517 polyacrylamide gels, then transferred to polyvinylidene difluoride (PVDF)
518 membranes (Millipore) using a semi-dry transfer apparatus (Bio-Rad). Membranes
519 were blocked with 5% bovine serum albumin (BSA) for 1h at room temperature and
520 immunoblotting was performed overnight at 4°C with the primary antibodies (Table
521 S3), followed by incubation with secondary antibody conjugated to HRP (Jackson
522 ImmunoResearch). Signals were generated by enhanced chemiluminescence
523 (Millipore) and detected by luminescent image analyzer (GE imagination LAS 4000).
524
525 **Immunohistochemistry (IHC) and Immunofluorescence (IF) analyses**
526 IHC and IF stainings were performed using standard protocols. For IHC staining,
527 paraffin sections were dewaxed and rehydrated, followed by antigen retrieval through
528 boiling the tissue for 15 min in 10 mM citrate buffer, pH 6.0. Then, the Histostain

529 LAB-SA Detection kits (Invitrogen) were applied according to the manufacturer's
530 instructions, and the sections were stained using DAB and nuclei were counterstained
531 with hematoxylin. Digital images were captured under a microscope (Olympus BX53)
532 equipped with an UPlanFN N 20×/0.5 objective (Olympus).

533 For IF staining, frozen 8-μm thick sections were prepared and then fixed with 4%
534 paraformaldehyde for 20 min at 4°C. The unspecific binding sites were blocked with
535 10% BSA/PBS for 60 min at room temperature, and sections were incubated with the
536 primary antibodies (Table S3) overnight at 4°C. Then, fluorescent-labeled secondary
537 antibodies (1:500, donkey anti–rabbit Alexa Fluor 488, donkey anti–mouse Alexa
538 Fluor 488, or donkey anti–rabbit Alexa Fluor 555, donkey anti–mouse Alexa Fluor
539 555, Jackson ImmunoResearch) were used. Nuclei were counterstained with DAPI
540 (Sigma-Aldrich). The fluorescence signals were detected under a laser scanning
541 confocal microscope (Carl Zeiss LSM-510, Germany) equipped with an argon laser
542 (488 nm), a He/Ne laser (543 nm), an EC Plan-NEOFLUAR 63×/1.25 objective and a
543 LD LCI Plan-APOCHROMAT 25×/0.8 objective (Zeiss). Digital images were
544 captured and processed using Aim software (Zeiss Systems).

545

546 **Cell cycle analysis**

547 Rate of germ cell development during spermatogenesis was studied in testis using
548 propidium iodide (PI) staining combined with flow cytometer analysis, which
549 resolved cell types based on differences in their DNA content. Briefly, the testes were
550 incubated in 1 ml PBS containing 1 mg/ml collagenase (Type IV; Sigma) at 37 °C for

551 30 min with gentle agitation. After sedimentation for 5 min, the supernatant was
552 removed and the seminiferous tubules were collected. Then, the seminiferous tubules
553 were digested in accutase cell dissociation reagent (Innovative Cell Technologies) for
554 15 min and the samples were passed through a nylon filter followed by centrifugation
555 at 400 xg for 5 min at room temperature. Thereafter, the pellet was re-suspended with
556 0.5 ml PBS-E (1 mM EDTA in PBS) and fixed with ice-cold 70% ethanol overnight at
557 4°C. The cells were permeabilized followed by staining with 0.5 mL PI/ribonuclease
558 staining buffer (BD Biosciences) and incubated at room temperature for 15 min in the
559 dark. Finally, DNA content of PI stained cells was analyzed in a flow cytometer
560 (Beckman Coulter CytoFlex S) equipped with a 561nm laser. In each sample, 50,000
561 events were recorded and further analyzed by Cytepert software (Beckman Coulter).
562 Three different cell populations were resolved in seminiferous tubules: 1N
563 (spermatids), 2N (spermatogonia, secondary spermatocytes and Sertoli cells) and 4N
564 (primary spermatocytes), and their ratios were calculated.
565
566 **BTB assay**
567 In vivo BTB assay was performed as described (Holembowski et al., 2014). Biotin
568 labeled reagent (10 mg/ml Sulfo-NHS-SS-Biotin, Thermo Scientific) was freshly
569 prepared in PBS containing 1 mM $CaCl_2$, and then 25 µl of this solution were
570 carefully injected into the center of the testis at low pressure. The contralateral testis
571 was injected with the same volume of calcium chloride solution alone and served as a
572 negative control. After 30 min exposure to biotin, the animals were euthanized, and

573 the testes were harvested and fixed in 10% neutral buffered formalin. Testis sections
574 were probed sequentially with Alexa Fluor 488 conjugated Streptavidin (Jackson
575 ImmunoResearch) to evaluate the extracellular distribution of biotin within the
576 seminiferous epithelium. Finally, the fluorescence signal was captured under a laser
577 scanning confocal microscope (Carl Zeiss LSM-510) equipped with an argon laser
578 (488 nm) and a LD LCI Plan-APOCHROMAT 25×/0.8 objective (Zeiss).
579
580 **Primary Sertoli cell culture**
581 Primary Sertoli cell culture was carried out as described (Sato et al., 2013;
582 Holembowski et al., 2014) with some modifications. Briefly, to obtain Sertoli cells for
583 primary culture, testes of adult mice were decapsulated in HBSS and seminiferous
584 tubules were dispersed in a HBSS solution containing collagenase
585 (0.1%)/hyaluronidase (0.1%)/DNase (0.04%) for 20 min at 34°C. After washing with
586 PBS, an additional digestion step was performed with accutase cell dissociation
587 reagent (Innovative Cell Technologies) for 15 min at 34°C. The tubular pellet was
588 washed with PBS and Sertoli cells were freed from the seminiferous epithelium by
589 resuspending the pellet in DMEM/F12 medium. Cells in the supernatant were
590 collected and cultured in DMEM/F12 medium containing 5% FBS overnight at 34°C.
591 Following attachment of the Sertoli cells to the bottom of the tissue culture plate, they
592 acquired an irregular shape, whereas the germ cells remained suspended and were
593 easily removed by repeated washing. The purity of primary Sertoli cells was routinely
594 analyzed by immunofluorescent staining with SOX9.

595

596 **Endocytosis assay**

597 Endocytosis was evaluated as described previously (Le et al., 1999). Briefly, cell
598 surface proteins were biotinylated with 0.5 mg/ml Sulfo-NHS-SS-Biotin (Pierce) in
599 PBS containing 0.9 mM $CaCl_2$ and 0.33 mM $MgCl_2$ at 4 °C for 30 min, and then
600 quenched with 50 mM NH_4Cl in PBS at 4 °C for 15 min and subsequently, incubated
601 at 34 ℃ for the indicated periods of time during which endocytosis occurred.
602 Biotinylated cargo proteins were then stained with Streptavidin-coupled FITC
603 (Jackson) and detected under a laser scanning confocal microscope (Carl Zeiss
604 LSM-510) equipped with an argon laser (488 nm) and an EC Plan-NEOFLUAR
605 63×/1.25 objective (Zeiss).

606

607 **Protein Immunoprecipitation (IP) and mass spectrometry (MS) assay**

608 Protein immunoprecipitation was characterized using the Pierce Direct IP kit (Thermo
609 scientific) according to the manual instructions. The LC-MS analysis was performed
610 as described (Liu et al. 2015). All MS/MS spectra were searched using Proteome
611 Discoverer2.2 software against the mouse UniProt database. Two missing cleavage
612 sites were allowed. The tolerances of peptides and fragment ions were set at 6 ppm
613 and 0.5 Da, respectively.

614

615 **Statistical Analysis**

616 All data were analyzed using SAS 8.2 software, and results are presented as mean ±

SD. Group comparisons were made using Student's t-test where appropriate. One-way analysis of variance (ANOVA) test was used assuming a two-tail hypothesis with $P< 0.05$. Differences were considered statistically different when $P<0.05$.

Supplemental material

Fig. S1 immunofluorescent staining indicates that JMY was localized in both Sertoli cells and spermatids in the seminiferous epithelium. Fig. S2 illustrates the gene engineering scheme used to obtain mice with conditional deletion of *Jmy*. Fig. S3 shows the COG analysis of proteins that immunoprecipitated with JMY. Fig. S4 shows that the testicular morphology, litter size and sperm parameters are normal in germ cell-specific deletion of *Jmy* (*Jmy* flox; *Mvh* cre) male mice. Table S1 shows results of the MS analysis of proteins immunoprecipitated with JMY. Table S2 shows the results of KEGG pathway analysis of proteins immunoprecipitated with JMY. Table S3 lists the primary antibodies used in this study.

Acknowledgments

The authors thank Ms.Yanqin Hu (Shanghai Key Laboratory for Reproductive Medicine) for her technical assistance in histological analysis and also thank Ms. Rong Fu (Core Facility of Basic Medical Sciences) for her technical assistance in flow cytometry assay. The authors are grateful to Prof. Peter Reinach for his editorial assistance.

This research project was supported by grants from the National Natural Science

Foundation of China (No. 81701503, No. 81370752 and No. 81571487) and Science and Technology Commission of Shanghai Municipality (No. 16ZR1418600).

Author contributions

Y. Liu conducted and performed experiments, analyzed data, and prepared the manuscript. J. Fan performed the animal experiments and analyzed the data. Y. Yan, X. Dang, R. Zhao and Y. Xu performed part of molecular experiments. Z. Ding designed and supervised the project, and provided final approval of the manuscript.

Conflict of interest

The authors declare that there is no conflict of interest that would prejudice the impartiality of this work. The authors also declare no competing financial interests.

Abbreviations

ARP3, actin-related protein 3; BTB, blood–testis barrier; CKO, conditional knock out; DHT, dihydrotestosterone; EEA-1, early endosomal antigen; ES, ectoplasmic specialization; H&E, hematoxylin and eosin; IP, immunoprecipitation; MS, mass spectrometry; JMY, junction-mediating and regulatory protein; Sorbs2, Sorbin and SH3 domain containing protein 2; ZO-1, zonula occludens-1.

References

Anekal, P.V., J. Yong, and E. Manser. 2015. Arg kinase-binding protein 2 (ArgBP2)

661 interaction with α-actinin and actin stress fibers inhibits cell migration. *J. Biol.*
662 *Chem.* 290:2112-2125.
663 Aristaeus de Asis, M., M. Pires, K. Lyon, and A.W. Vogl. 2013. A network of spectrin
664 and plectin surrounds the actin cuffs of apical tubulobulbar complexes in the rat.
665 *Spermatogenesis.* 3:e25733.
666 Chen, H., M.W.M. Li, and C.Y. Cheng. 2017. Drebrin and Spermatogenesis. *Adv. Exp.*
667 *Med. Biol.* 1006:291-312.
668 Cheng, C.Y., E.W. Wong, P.P. Lie, M.W. Li, D.D. Mruk, H.H. Yan, K.W. Mok, J.
669 Mannu, P.P. Mathur, W. Y. Lui, et al. 2011. Regulation of blood-testis barrier
670 dynamics by desmosome, gap junction, hemidesmosome and polarity proteins:
671 An unexpected turn of events. *Spermatogenesis*. 1:105-115.
672 Cheng, C.Y., P.P. Lie, E.W. Wong, D.D. Mruk, and B. Silvestrini. 2011. Adjudin
673 disrupts spermatogenesis via the action of some unlikely partners: Eps8, Arp2/3
674 complex, drebrin E, PAR6 and 14-3-3. *Spermatogenesis.* 1:291-297.
675 Chojnacka, K., B. Bilinska, and D.D. Mruk. 2017. Annexin A2 is critical for
676 blood-testis barrier integrity and spermatid disengagement in the mammalian
677 testis. *Biochim. Biophys. Acta.* 1864:527-545.
678 Coutts, A.S., L. Weston, and N.B. La Thangue. 2009. A transcription co-factor
679 integrates cell adhesion and motility with the p53 response. *Proc. Natl. Acad. Sci.*
680 *U S A.* 106:19872-19877.
681 Du, M., J. Young, M. De Asis, J. Cipollone, C. Roskelley, Y. Takai, P.K. Nicholls, P.G.
682 Stanton, W. Deng, B.B. Finlay, et al. 2013. A novel subcellular machine

683 contributes to basal junction remodeling in the seminiferous epithelium. *Biol.*
684 *Reprod.* 88:60.
685 França, L.R., R.A. Hess, J.M. Dufour, M.C. Hofmann, and M.D. Griswold. 2016. The
686 Sertoli cell: one hundred fifty years of beauty and plasticity. *Andrology.*
687 4:189-212.
688 Griswold, M.D. 1998. The central role of Sertoli cells in spermatogenesis. *Semin. Cell*
689 *Dev. Biol.* 9:411-416.
690 Griswold, M.D. 2018. 50 years of Spermatogenesis: Sertoli cells and their Interactions
691 with Germ Cells. *Biol. Reprod.* doi: 10.1093/biolre/ioy027.
692 Guttman, J.A., P. Janmey, and A.W. Vogl. 2002. Gelsolin--evidence for a role in
693 turnover of junction-related actin filaments in Sertoli cells. *J. Cell Sci.*
694 115:499-505.
695 Holembowski, L., D. Kramer, D. Riedel, R. Sordella, A. Nemajerova, M. Dobbelstein,
696 and U.M. Moll. 2014. TAp73 is essential for germ cell adhesion and maturation
697 in testis. *J. Cell Biol.* 204:1173-1190.
698 Jia, X., Y. Xu, W. Wu, Y. Fan, G. Wang, T. Zhang, and W. Su. 2017. Aroclor1254
699 disrupts the blood-testis barrier by promoting endocytosis and degradation of
700 junction proteins via p38 MAPK pathway. *Cell Death Dis.* 8:e2823.
701 Le, T.L., A.S. Yap, and J.L. Stow. 1999. Recycling of E-cadherin: a potential
702 mechanism for regulating cadherin dynamics. *J. Cell Biol.* 146:219-232.
703 Li, L., Y. Gao, H. Chen, T. Jesus, E. Tang, N. Li, Q. Lian, R.S. Ge, and C.Y. Cheng.
704 2017. Cell polarity, cell adhesion, and spermatogenesis: role of cytoskeletons.

F1000Res. 6:1565.

Li, M.W., X. Xiao, D.D. Mruk, Y.L. Lam, W.M. Lee, W.Y. Lui, M. Bonanomi, B. Silvestrini, and C.Y. Cheng. 2011. Actin-binding protein drebrin E is involved in junction dynamics during spermatogenesis. *Spermatogenesis*. 1:123-136.

Li, N., D.D. Mruk, and C.Y. Cheng. 2015. Actin binding proteins in blood-testis barrier function. *Curr. Opin. Endocrinol. Diabetes Obes.* 22:238-247.

Li, N., E.I. Tang, and C.Y. Cheng. 2016. Regulation of blood-testis barrier by actin binding proteins and protein kinases. *Reproduction.* 151:29-41.

Lie, P.P., A.Y. Chan, D.D. Mruk, W.M. Lee, and C.Y. Cheng. 2010. Restricted Arp3 expression in the testis prevents blood-testis barrier disruption during junction restructuring at spermatogenesis. *Proc. Natl. Acad. Sci. U S A.* 107:11411-11416.

Liu, J.J. 2016. Retromer-Mediated Protein Sorting and Vesicular Trafficking. *J. Genet. Genomics*. 43:165-177.

Liu, Y., Y. Guo, N. Song, Y. Fan, K. Li, X. Teng, Q. Guo, and Z. Ding. 2015. Proteomic pattern changes associated with obesity-induced asthenozoospermia. *Andrology.* 3:247-259.

Lui, W.Y., W.M. Lee, and C.Y. Cheng. 2003. Sertoli-germ cell adherens junction dynamics in the testis are regulated by RhoB GTPase via the ROCK/LIMK signaling pathway. *Biol. Reprod.* 68:2189-2206.

Mital, P., B.T. Hinton, and J.M. Dufour. 2011. The blood-testis and blood-epididymis barriers are more than just their tight junctions. *Biol. Reprod.* 84:851-858.

Mok, K.W., H. Chen, W.M. Lee, and C.Y. Cheng. 2015. rpS6 regulates blood-testis

727 barrier dynamics through Arp3-mediated actin microfilament organization in rat
728 sertoli cells. An in vitro study. *Endocrinology.* 156:1900-1913.
729 Mruk, D.D., and C.Y. Cheng. 2004. Sertoli-Sertoli and Sertoli-germ cell interactions
730 and their significance in germ cell movement in the seminiferous epithelium
731 during spermatogenesis. *Endocr. Rev.* 25:747-806.
732 Mruk, D.D., and C.Y. Cheng. 2015. The Mammalian Blood-Testis Barrier: Its Biology
733 and Regulation. *Endocr. Rev.* 36:564-591.
734 Murphy, A.C., and P.W. Young. 2015. The actinin family of actin cross-linking
735 proteins - a genetic perspective. *Cell Biosci.* 5:49.
736 Papadopulos, A. 2017. Membrane shaping by actin and myosin during regulated
737 exocytosis. *Mol. Cell Neurosci*. 84:93-99.
738 Roadcap, D.W., and J.E. Bear. 2009. Double JMY: making actin fast. Nat. Cell Biol.
739 11:375-376.
740 Roignot, J., and P. Soubeyran. 2009. ArgBP2 and the SoHo family of adapter proteins
741 in oncogenic diseases. *Cell Adh. Migr.* 3:167-170.
742 Rönty, M., A. Taivainen, M. Moza, G.D. Kruh, E. Ehler, and O. Carpen. 2005.
743 Involvement of palladin and alpha-actinin in targeting of the Abl/Arg kinase
744 adaptor ArgBP2 to the actin cytoskeleton. *Exp. Cell Res*. 310:88-98.
745 Rottner, K., J. Hänisch, and K.G. Campellone. 2010. WASH, WHAMM and JMY:
746 regulation of Arp2/3 complex and beyond. *Trends Cell Biol*. 20:650-661.
747 Sato, Y., K. Yoshida, S. Nozawa, M. Yoshiike, M. Arai, T. Otoi, and T. Iwamoto. 2013.
748 Establishment of adult mouse Sertoli cell lines by using the starvation method.

Reproduction. 145:505-516.

Stanton, P.G. 2016. Regulation of the blood-testis barrier. *Semin. Cell Dev. Biol.* 59:166-173.

Su, L., D.D. Mruk, W.M. Lee, and C.Y. Cheng. 2010. Differential effects of testosterone and TGF-β3 on endocytic vesicle-mediated protein trafficking events at the blood-testis barrier. *Exp. Cell Res.* 316:2945-2960.

Vogl, A.W., M. Du, X.Y. Wang, and J.S. Young. 2014. Novel clathrin/actin-based endocytic machinery associated with junction turnover in the seminiferous epithelium. *Semin. Cell Dev. Biol.* 30:55-64.

Xiao, X., D.D. Mruk, E.I. Tang, R. Massarwa, K.W. Mok, N. Li, C.K. Wong, W.M. Lee, S.B. Snapper, B.Z. Shilo, et al. 2014. N-wasp is required for structural integrity of the blood-testis barrier. *PLoS Genet.* 10:e1004447.

Yan, H.H., D.D. Mruk, W.M. Lee, and C.Y. Cheng. 2008. Blood-testis barrier dynamics are regulated by testosterone and cytokines via their differential effects on the kinetics of protein endocytosis and recycling in Sertoli cells. *FASEB J.* 22:1945-1959.

Zuchero, J.B., A.S. Coutts, M.E. Quinlan, N.B. Thangue, and R.D. Mullins. 2009. p53-cofactor JMY is a multifunctional actin nucleation factor. *Nat. Cell Biol.* 11:451-459.

Figure Legends

Figure 1. JMY expression in testis and Sertoli cells. (A) JMY Immunofluorescent

771 staining shows that JMY expression is localized in the Sertoli cells of mouse testis
772 (Arrows indicated). Bars: (main) 50 μm; (enlarged) 20 μm. (B) JMY
773 immunofluorescent staining and F-actin rhodamine-phalloidin staining of primary
774 cultured Sertoli cells shows that its expression is localized in the cytosol and nucleus.
775 In the cytosol, JMY has a filamentous distribution, which in some places colocalizes
776 with F-actin. Scale Bar: 20μm.
777
778 **Figure 2. WT and *Jmy* CKO sperm morphology analyses.** (A) Western blot
779 analysis resolves JMY expression in mouse testicular Sertoli cells. JMY expression
780 was greatly reduced in CKO testis relative to that in its WT counterpart and Het testis,
781 JMY expression was undetectable in Sertoli cells of CKO mice. GAPDH expression
782 validated loading equivalence. (B) JMY immunofluorescent staining of shows that
783 JMY expression in Sertoli cells was absent in testis from *Jmy* CKO mice. Scale Bar:
784 50 μm. (C) Litter size of mature female mice mated with *Jmy* CKO male mice was
785 greatly reduced relative to those mated with WT and Het male mice. Error bars
786 represent SD (n=10). $^{**}P < 0.01$. (D) Sperm motility analyzed by CASA shows that
787 both sperm motility and progressive motility of *Jmy* CKO mice were less than that in
788 WT and Het mice. Error bars represent SD (n=5). $^{*}P < 0.05$; $^{**}P < 0.01$. (E) Sperm
789 concentration analyzed by CASA, shows that sperm concentration of *Jmy* CKO mice
790 was lower than that in WT and Het mice. Error bars represent SD (n=5). $^{*}P < 0.05$. (F)
791 Sperm morphology of WT and *Jmy* CKO mice. Except for the prominent
792 deformations in the *Jmy* CKO sperm heads, the other regions appear unchanged from

the normal WT morphology (CKO, arrows indicated). Bars: (main) 50 μm; (enlarged) 20 μm. (G) Deformed sperm head ratios calculated from five independent experiments of at least 200 spermatozoa in each independent experiment. Error bars represent SD (n=5). $^{**}P < 0.01$.

Figure 3. Loss of JMY function induces testicular histological disorder. (A-B) In H&E stained testicular (A) and caput epididymal (B) sections, testicular cellular disorganization is evident and spermatid epithelial adherence is less. These alterations obstruct caput epididymis lumen patency in *Jmy* CKO mice. Bars: (main) 100 μm; (enlarged) 50 μm. (C) Cell cycle analysis results resolve different cell types in the seminiferous epithelium. DNA content of indicated cell types: diploid (2N), tetraploid (4N) and haploid (N). Statistical results show that the proportion of haploid cells increased in *Jmy* CKO mice. Error bars represent SD (n = 5; 30,000 cells per test). $^{**}P < 0.01$. (D) Vimentin immunohistochemical staining is evident in testicular sections. Vimentin is one kind of intermediate filamentous protein that is an established marker of Sertoli cells. Sertoli cell numbers in every seminiferous tubule from WT mice and *Jmy* CKO mice are not significantly different from one another. Error bars represent SD (n = 30; 5 tubules/trial). (E-F) Transmission electron micrograph analysis of seminiferous epithelium shows that spermatid cell adhesions are incomplete within the seminiferous epithelium of *Jmy* CKO testes (E) which are accompanied by disrupted junctional structures between neighboring Sertoli cells (F). Arrows in (F) indicate the actin bundles of the ES in WT mice. Bars: (E) 10 μm; (F) 2

μm; (zoom in F) 0.2 μm. (G) The biotin assay evaluated BTB integrity in vivo. Alexa Fluor 488 staining visualized biotin distribution. The diffuse green fluorescent staining throughout all the layers of the testicular seminiferous epithelium indicates that loss of JMY function contributes to defective BTB structural formation in the he *Jmy* CKO mice. Scale Bar: 100 μm.

Figure 4. Loss of JMY function disrupts cell junctional integrity between testicular Sertoli cells. (A) Comparison of Western blot analyses of testicular protein expression in WT and *Jmy* CKO mice. Clathrin and EEA-1, endocytosis related proteins; ZO-1, β-catenin, N-cadherin and Claudin11 expressions identified junctional proteins; Vimentin and GAPDH expression validated loading control equivalence. (B) Immunohistochemical staining of testicular sections, junctional Claudin11 and N-cadherin proteins, shows that their expression is localized to the basolateral region of adjacent Sertoli cells in WT testes. In contrast, such delimited junctional expression is not evident in *Jmy* CKO testicular Sertoli cells. Scale Bar: 50 μm. (C) Western blot analyses of proteins expression patterns in WT Sertoli cells and *Jmy* CKO Sertoli cells, as well as in those treated with either DHT or Dynasore. Vimentin and GAPDH expression validated loading control equivalence. (D) Immunofluorescent staining of junction proteins (N-cadherin and ZO-1) and endocytosis related proteins (Caveolin-1 and Clathrin), shows decreased amount of N-cadherin and ZO-1 expression whereas caveolin-1 and clathrin expression increased in the *Jmy* CKO Sertoli cells. Scale Bar: 50 μm.

837

838 **Figure 5. Endosome cycling disrupted in *Jmy* CKO Sertoli cells.** (A) Changes in
839 cell surface biotinylation evaluated endocytosis and recycling in Sertoli cells. After
840 biotin labeling for 0h, 1h and 3h, the intracellular translocation of the biotinylated
841 membrane proteins was detected by fluorescent staining. Bars: 20 μm. (B) Dynasore
842 treatment blocked endocytosis, which resulted in less cytoplasmic biotinylated protein
843 accumulation in the cytoplasm. Bars: 20 μm. (C) The contribution by functional JMY
844 expression to mediating endocytosis of biotinylated membrane proteins was evaluated
845 based on its co-localization with endosomal biomarkers. In Jmy CKO Sertoli cells,
846 immunofluorescent staining shows that the biotinylated membrane proteins
847 accumulated in the cytoplasm and co-localized with endocytic vesicle markers
848 (clathrin and caveolin), whereas less biotinylated proteins co-localized with
849 endosomal protein markers (EEA-1 and Rab 11). Scale Bars: 20 μm.

850

851 **Figure 6. Identification of the proteins interacting with JMY in Sertoli cells.** (A)
852 Proteins coimmunoprecipating with JMY antibodies are evident in Western blots
853 interrogated with α-actinin1 and Sorbs2 antibodies in a protein lysate of Sertoli cells
854 expressing JMY. (B) Immunofluorescent staining identifies co-localization of JMY
855 with either α-actinin1 or Sorbs2 in Sertoli cells. Scale Bars: (main) 20 μm; (zoom) 5
856 μm

857

858 **Figure 7. Loss of JMY function disrupts interactions between actin filament and**

actin regulating proteins in Sertoli cells. (A) Rhodamine-phalloidin staining identified numerous actin filaments foci in *Jmy* CKO Sertoli cells (Arrows highlight). Scale Bars: (main) 50 μm; (enlarged) 20 μm. (B) Western blot analyses of α-Actinin and Sorbs2 expression show that their expression levels are slightly less in *Jmy* CKO Sertoli cells than in the WT counterpart, but that of Arp3 is unchanged in *Jmy* CKO Sertoli cells. Vimentin and ß-actin expression levels document loading control equivalence. (C) Localized Arp3, actinin1 and Sorbs2 immunofluorescent staining in WT Sertoli cells and *Jmy* CKO Sertoli cells. Arp3, actinin1 and Sorbs2 colocalize with actin filaments in WT Sertoli cells whereas their close proximity to one another is lost in *Jmy* CKO Sertoli cells. Scale Bars: 20 μm.

Tables and their legends

Table S1. MS identification of proteins immunoprecipitated with JMY

Table S2. KEGG pathway analysis of proteins immunoprecipitated with JMY

Table S3. Primary antibodies used in this study

Figure S1. JMY localization in mouse testis. JMY immunofluorescent staining was selective and evident in the seminiferous epithelium (A). The staining was greatly localized to the Sertoli cells (B) and in the post acrosomal region of spermatids in close proximity to the manchette structure (C). Arrows indicate JMY immunofluorescent staining in Sertoli cells (B) or spermatids (C). Scale Bars: (A) 50 μm; (B and C) 20 μm.

881

882 **Figure S2. Scheme of engineering *Jmy* Sertoli cell CKO mice**. Two loxP sites were
883 inserted into both sides of the third exon in the *Jmy* gene using homologous
884 recombination. Specific deletion of *Jmy* was carried out by a Sertoli cell specific
885 expression of Cre recombinase.

886

887 **Figure S3. Orthologous groups of proteins clusters (COG) identified based on**
888 **analysis of proteins coprecipitating with JMY in Sertoli cells.**

889

890 **Figure S4. Germ cell fertility unaltered by loss of *Jmy* function.** Male germ cell
891 fertility is unaffected in *Jmy* CKO (A-C) Litter size (A), Sperm concentration (B) and
892 Sperm motility (C). *Jmy* CKO male mice (*Jmy* flox; *Mvh* cre) germ cell fertility is
893 similar to those in WT male mice. Error bars represent SD (n=5). (D) H&E stained
894 testicular sections indicate no significant change in histological structure and integrity
895 in *Jmy* CKO testis (n = 3). Scale Bars: (main) 100 μm; (enlarged) 50 μm.

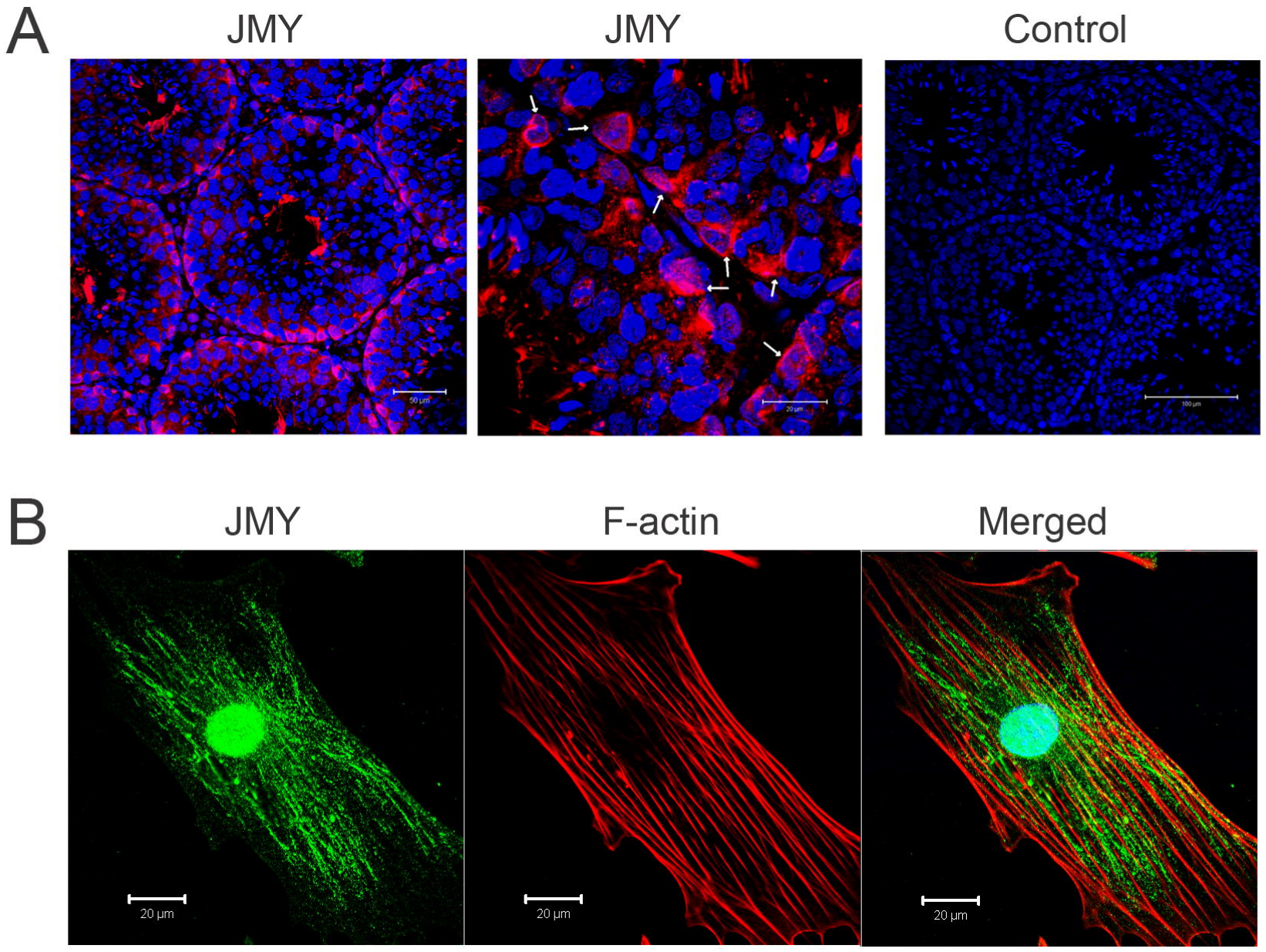
A
JMY
JMY
Control
50 µm
20 µm
100 µm
B
JMY
F-actin
Merged
20 µm
20 µm
20 µm

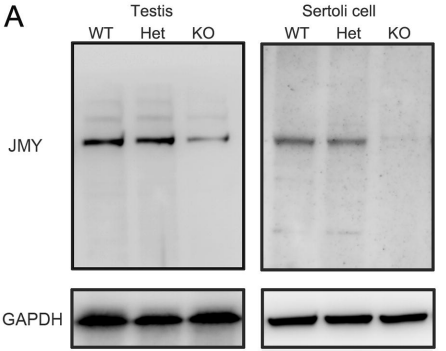
A
Testis
WT
Het
KO
Sertoli cell
WT
Het
KO
JMY
GAPDH

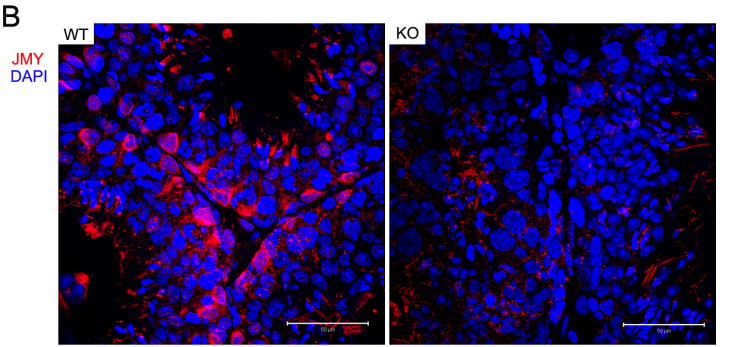
B
WT
KO
JMY
DAPI

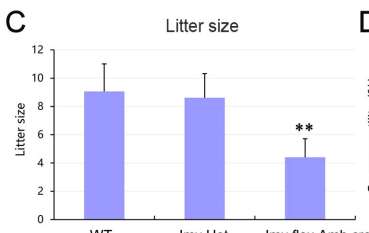
C
Litter size
Litter size
12
10
8
6
4
2
0
**
WT
Jmy Het
Jmy flox Amh cre

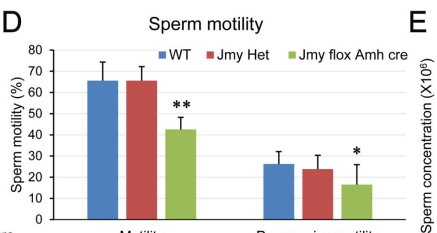
D
Sperm motility
WT
Jmy Het
Jmy flox Amh cre
Sperm motility (%)
80
70
60
50
40
30
20
10
0
**
*
Motility
Progressive motility

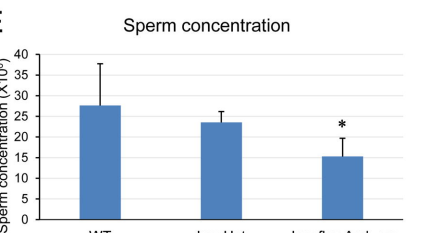
E
Sperm concentration
Sperm concentration (X10⁶)
40
35
30
25
20
15
10
5
0
*
WT
Jmy Het
Jmy flox Amh cre

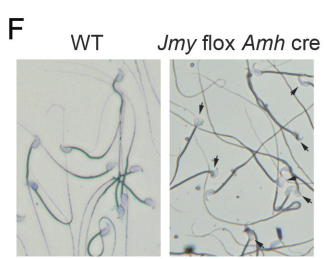
F
WT
Jmy flox Amh cre
50 μm

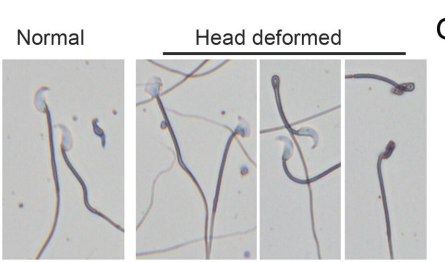
Normal
Head deformed
20 μm

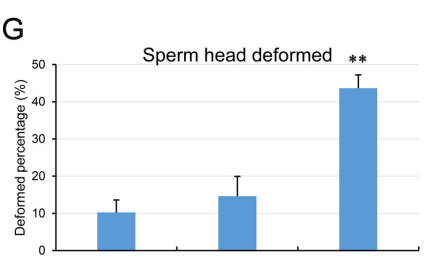
G
Sperm head deformed
Deformed percentage (%)
50
40
30
20
10
0
**
WT
Jmy Het
Jmy flox Amh cre+

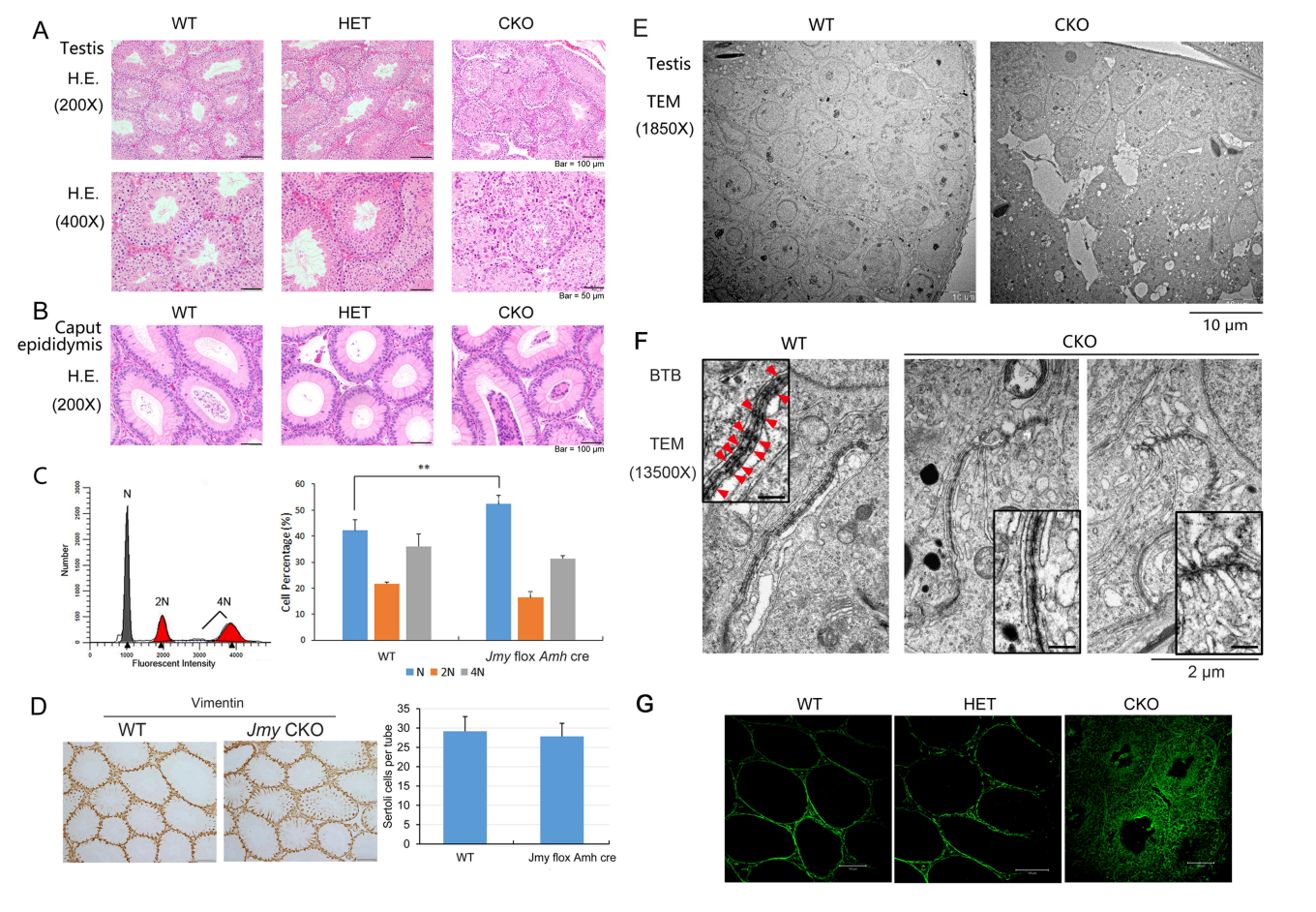
A
WT
HET
CKO
Testis
H.E.
(200X)
Bar = 100 μm
H.E.
(400X)
Bar = 50 μm
B
Caput epididymis
H.E.
(200X)
Bar = 100 μm
C
N
2N
4N
Number
Fluorescent Intensity
**
Cell Percentage (%)
WT
Jmy flox Amh cre
N 2N 4N
D
Vimentin
WT
Jmy CKO
Sertoli cells per tube
WT
Jmy flox Amh cre
E
WT
CKO
Testis
TEM
(1850X)
10 μm
F
WT
CKO
BTB
TEM
(13500X)
2 μm
G
WT
HET
CKO

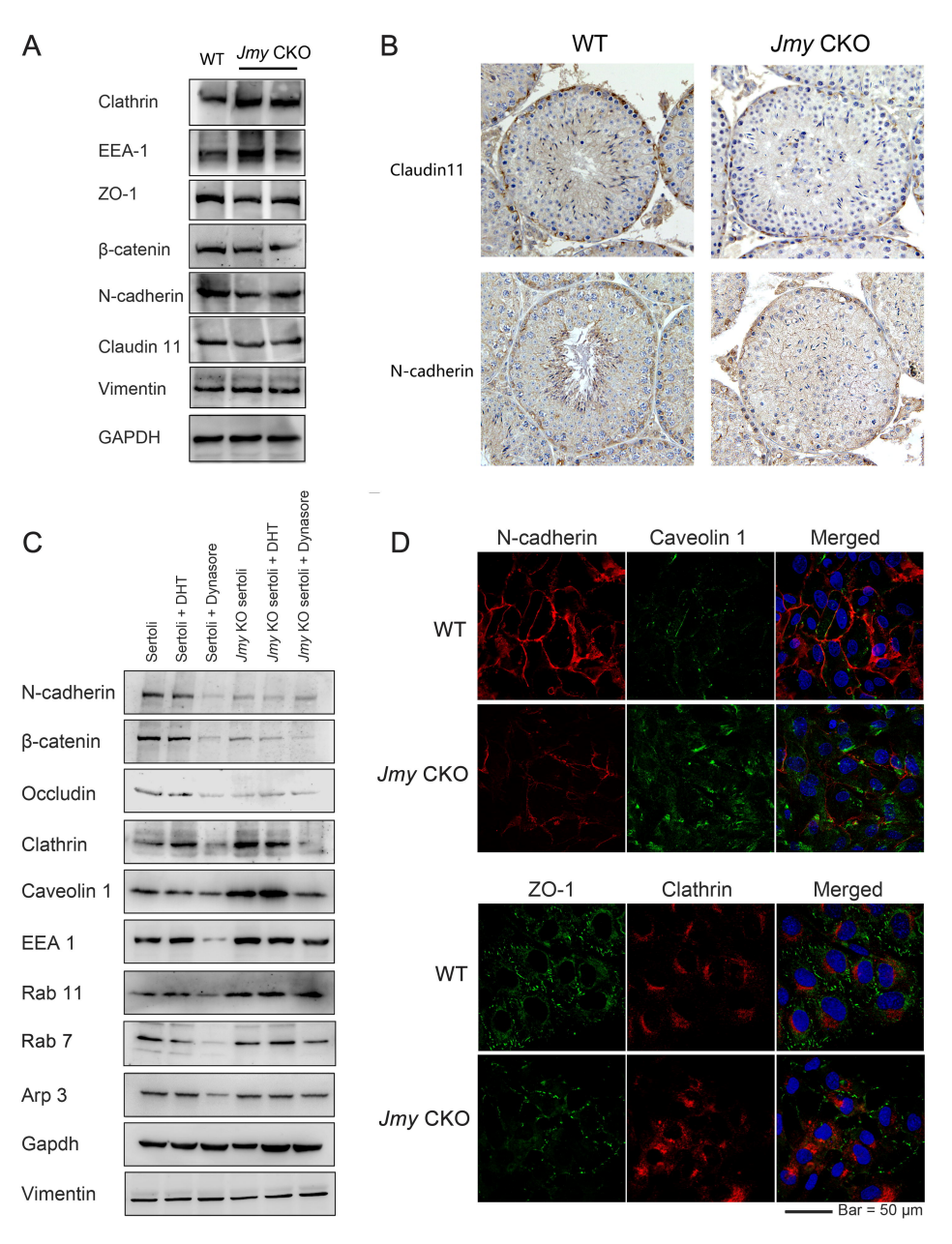
A
WT
Jmy CKO
Clathrin
EEA-1
ZO-1
β-catenin
N-cadherin
Claudin 11
Vimentin
GAPDH
B
WT
Jmy CKO
Claudin11
N-cadherin
C
Sertoli
Sertoli + DHT
Sertoli + Dynasore
Jmy KO sertoli
Jmy KO sertoli + DHT
Jmy KO sertoli + Dynasore
N-cadherin
β-catenin
Occludin
Clathrin
Caveolin 1
EEA 1
Rab 11
Rab 7
Arp 3
Gapdh
Vimentin
D
N-cadherin
Caveolin 1
Merged
WT
Jmy CKO
ZO-1
Clathrin
Merged
WT
Jmy CKO
Bar = 50 μm

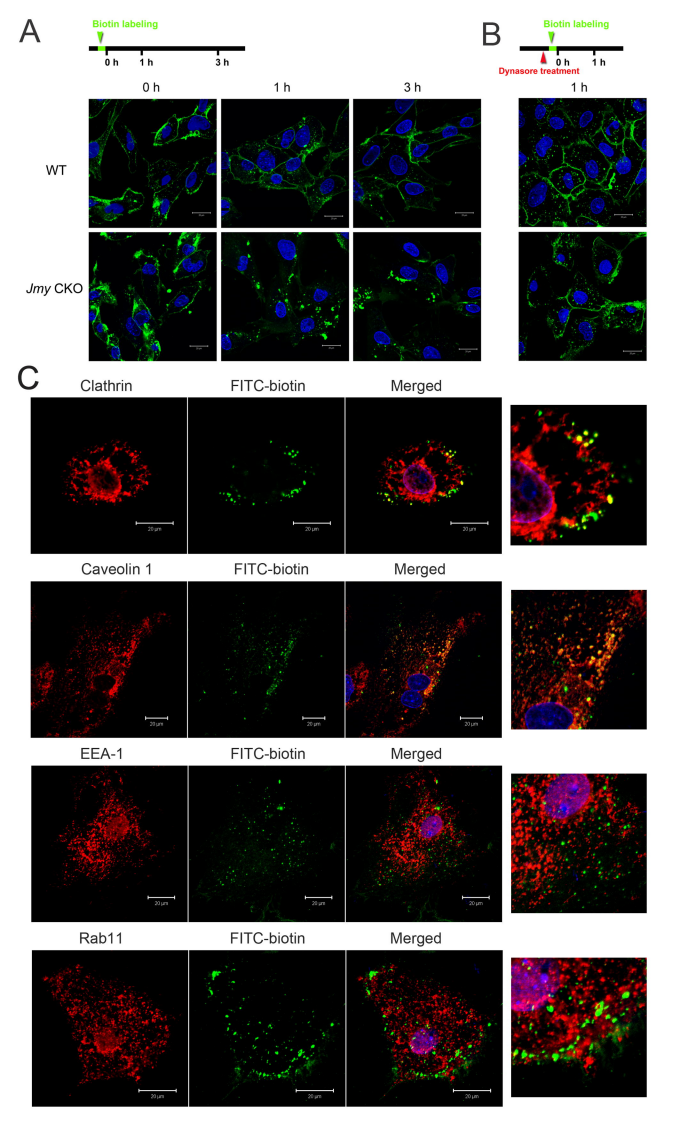
A
Biotin labeling
0 h
1 h
3 h
B
Biotin labeling
0 h
1 h
Dynasore treatment
0 h
1 h
3 h
1 h
WT
Jmy CKO
C
Clathrin
FITC-biotin
Merged
Caveolin 1
FITC-biotin
Merged
EEA-1
FITC-biotin
Merged
Rab11
FITC-biotin
Merged

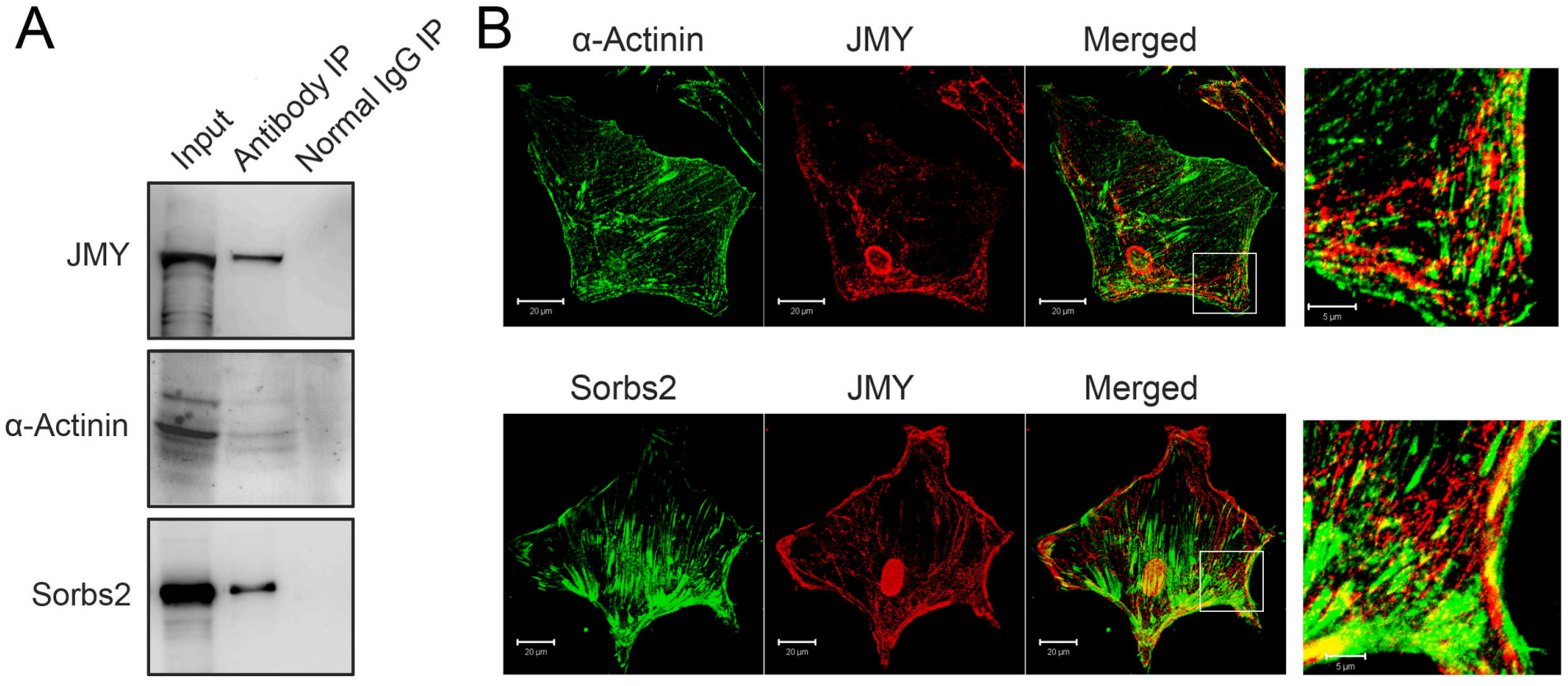
A
Input
Antibody IP
Normal IgG IP
JMY
α-Actinin
Sorbs2
B
α-Actinin
JMY
Merged
Sorbs2
JMY
Merged
20 μm
5 μm

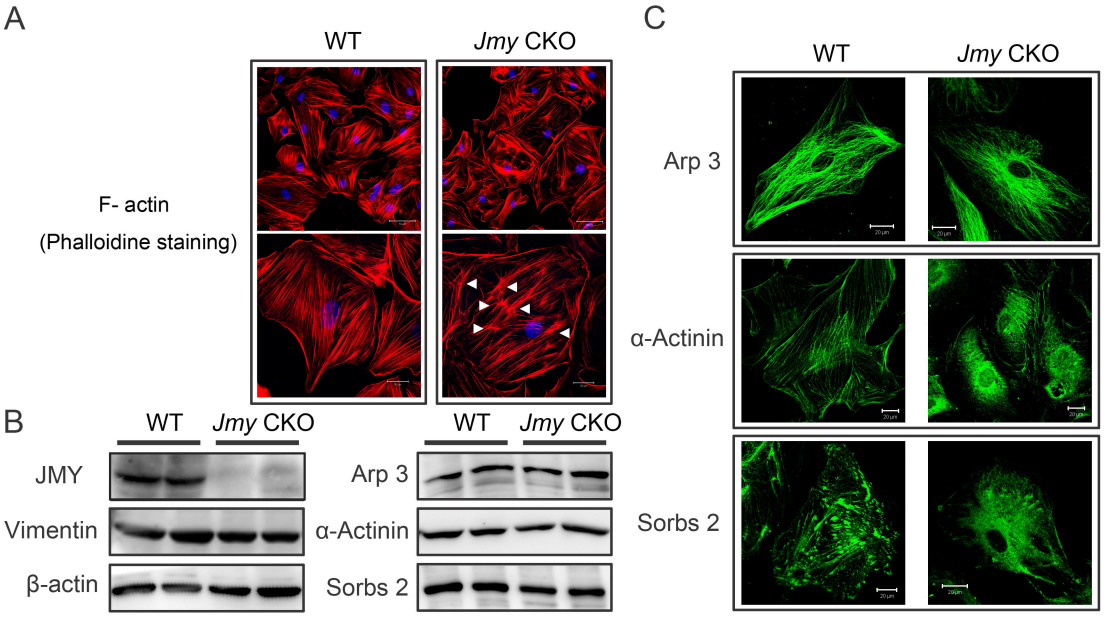
A
WT
Jmy CKO
F- actin
(Phalloidine staining)
B
WT
Jmy CKO
JMY
Vimentin
β-actin
WT
Jmy CKO
Arp 3
α-Actinin
Sorbs 2
C
WT
Jmy CKO
Arp 3
α-Actinin
Sorbs 2